Aluminum Cladding Oxide Growth Prediction for High Flux Research Reactors

Yeon Soo Kim [a,*], H.T. Chae [b], S. Van den Berghe [c], A. Leenaers [c], V. Kuzminov [c], A.M. Yacout [a]

a: Argonne National Laboratory, 9700 South Cass Avenue, Argonne, IL 60439 USA

b: Korea Atomic Energy Research Institute (KAERI)

989-111 Daedeok-daero, Yuseong-gu, Daejeon 305-353 Republic of Korea

c: SCK.CEN, Boeretang 200, 2400 Mol Belgium

* Corresponding author, e-mail address: yskim@anl.gov

Phone: 630-252-3173

Aluminum Cladding Oxide Growth Prediction for High Flux Research Reactors

Yeon Soo Kim, H.T. Chae, S. Van den Berghe, A. Leenaers, V. Kuzminov, A.M. Yacout

ABSTRACT

Aluminum cladding oxidation of research-reactor fuel elements at high power conditions has a disadvantageous effect on fuel performance due to the lower thermal conductivity of the oxide. The oxide growth prediction models available in the literature were mostly developed for low power conditions. To examine the applicability of the models to high power and high temperature test conditions, the models were studied by coupling with the most frequently employed heat transfer coefficient (HTC) correlations including the Dittus-Boelter correlation, the Colburn correlation, the Sieder-Tate correlation, and KAERI-developed correlation. The Griess model over-predicted the oxide growth while the KAERI-Griess model under-predicted the oxide growth for high power tests. The Kim model, coupled with the Colburn correlation, gave most consistent results with the measured data from two BR2 experiments. However, the Kim model was found to be inapplicable to the EUHFRR conditions at the peak power locations if it was coupled with the Dittus-Boelter correlation. A revision of the prediction models to more closely agree with the measured data was recommended. AG3NE and AlFeNi cladding types were tested in the E-FUTURE experiment, and a noticeable (although small) reduction in oxide thickness on the AlFeNi cladding was observed. However, this difference was believed to be only a secondary effect considering other uncertainties in model predictions, so no attempt was made to model the alloying effect.

Keywords: aluminum alloy cladding, research reactor fuel plate, in-pile oxide data, oxide growth prediction model

1. Introduction

Aluminum alloys have been used for research reactor fuel cladding since its first use for the MTR in the 1950s. Because the main purpose of research and test reactors is to produce neutrons, rather than power, a cladding with a low neutron absorption cross section is desired. In spite of their low melting points, aluminum alloys have the desired low neutron absorption and have a high thermal conductivity.

Aluminum alloy cladding undergoes oxidation in water, developing a protective oxide layer (Al_2O_3). In time, the Al_2O_3 layer is degraded by the formation of oxide-hydrates such as boehmite ($Al_2O_3 \cdot H_2O$) and bayerite ($Al_2O_3 \cdot 3H_2O$). Typically, the boehmite takes the major part of the corrosion products and the bayerite is found at the outer surface of the boehmite layer. In the present work, the term 'oxide' generally includes these corrosion products.

In slightly acidic coolant, aluminum alloys are an excellent material choice as they are resistant to oxidation, and corrosion in general. Before LEU fuel was considered, the research reactors adopted dispersion fuel forms with sparsely dispersed HEU fuel kernels in an Al matrix. Hence, fuel temperatures were relatively low. In this situation, cladding oxidation was not a concern as long as the oxide film did not spall off. However, when LEU fuel was pursued for high power applications, more densely populated fuel kernels increase fuel temperature, so cladding oxidation became a critical factor. The aluminum oxide elevates the fuel temperature because it has a thermal conductivity that is about two orders of magnitude lower than aluminum. For example, a 10-μm thick oxide at a heat flux of 450 W/cm^2 increases the fuel temperature by approximately 20 ^{o}C. Therefore, excessive oxidation can potentially degrade fuel performance because higher fuel temperature is always disadvantageous for fuel performance. In this sense, using a corrosion resistant material for cladding is crucial, so is providing a reliable prediction model for oxidation growth for fuel design and performance analysis.

Since being published in the early 1960s, the Griess model has been most frequently used for oxide prediction for the aluminum alloy cladding adopted in research reactors [1][2], although other models have been developed later to modify the Griess model [3]-[5]. These models take into account different variables, but they are in common based upon out-of-pile data. The most recent modification of the Griess model was published at KAERI to be applicable to the HANARO reactor in 1994 [6]. In 2008, to overcome the narrow applicable ranges of the existing models, a more versatile oxide prediction model was developed at ANL using existing data from out-of-pile and in-pile tests [7]. Because of potential limitations of the power range (or specifically heat flux), different cladding alloy types, and different coolant channel geometry compared to the data used to develop the prediction models, a review of the existing models was necessary before application to high power research reactors, including the EU high flux research reactors (EUHFRR).

From the E-FUTURE and SELENIUM experiments, systematically measured oxide data were available [8][9]. These experiments were conducted on real-size fuel plates in the BR2 reactor for the purpose of development and qualification of UMo/Al dispersion fuel for EUHFRR at bounding power and burnup

conditions for the EUHFRR including BR2, RHF and JHR. The power and burnup conditions used in these tests were higher than those of the experiments from which the oxide data were obtained and used for the developing the oxide prediction models.

Because cladding temperature is one of the key factors for cladding oxidation, it is important to accurately predict the temperature increase at the plate surface for the EU experiments with demandingly high heat fluxes. The most frequently used heat transfer coefficient (HTC) correlations at the cladding surface were examined, incorporating detailed thermal-hydraulic properties. Cladding surface temperature was then calculated and used to predict the oxide thickness based on the available models.

The unique features of the full-size plate experiments may affect oxide growth kinetics. In addition, the effect of alloy types was also examined because the existing models were developed based on the measured data for mostly AA6061 whereas the EUHFRR uses AG3NE or AlFeNi.

The accurate fuel performance prediction of a code such as DART [10] and MAIA [11] would depend on the availability of an optimized cladding oxide growth model in predicting fuel temperature that has an effect on fuel microstructural evolution. It would be possible to benchmark between codes when they can use the same oxide growth model in comparing more efficiently calculated and measured values describing the meat microstructure evolution under irradiation [12].

2. Experimental data

2.1 High power experiments at BR2

The E-FUTURE experiment at the BR2 consisted of four full-size flat plates in a dedicated irradiation basket [8]. Two different cladding types were tested; AG3NE as used in BR2 and AlFeNi as used in RHF. The coolant enters at the top of the test basket with downward flow. Before the start of the last irradiation cycle, plate 6111 was rotated 180^{o} along the length axis, which exposed this plate to uniquely different conditions from the other plates (and atypical to the expected conditions of the final fuel design). Therefore, we decided to exclude this plate from the evaluation, so only 6301, 4111, and 4202 plates were examined. Table 1 shows the irradiation data for the E-FUTURE experiment.

The SELENIUM experiment included two full-size plates in the same basket that was used for the E-FUTURE experiment; one plate on each side of the center divider with aluminum dummy plates in the remaining positions [9]. The plate 1221 that had available measured oxide data was examined in this study. The test plate dimensions were also designed to be the same as the E-FUTURE experiment. The cladding type for the SELENIUM experiment was AG3NE. The test conditions were similar to the E-FUTURE experiment (see Table 1).

A schematic cross-section view of the test basket and the fuel plates for both experiments are shown in **Figure 1** and **Figure 2**, respectively [8][9].

Table 1 Irradiation conditions for the E-FUTURE and SELENIUM experiments

	Cycle 1	Cycle 2	Cycle 3
Duration (d): E/S	26/21	31/27	20/21
Peak heat flux (W/cm^2): E/S	472/466	336/389	318/294
Coolant inlet temperature (^{o}C): C	38	38	38
Coolant speed in basket (m/s): C	12	12	12
Coolant pH: C	6.2	6.2	6.2

E = E-FUTURE, S = SELENIUM, C = common for both experiments

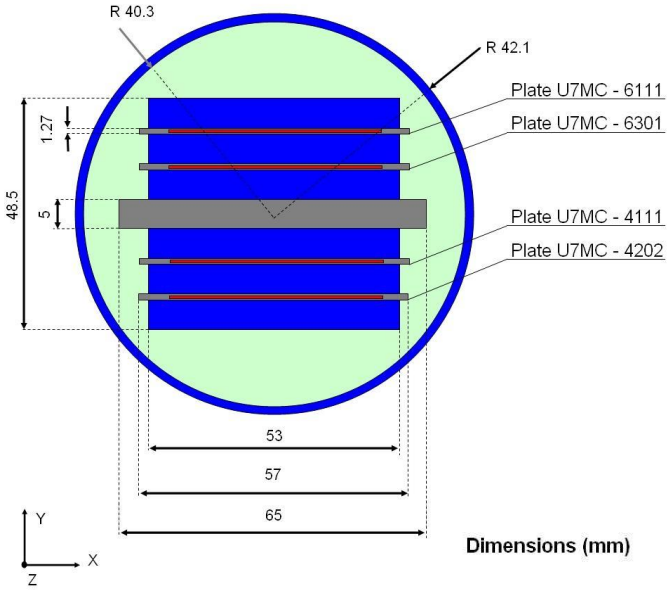

Figure 1 Schematic of the cross section of the test basket

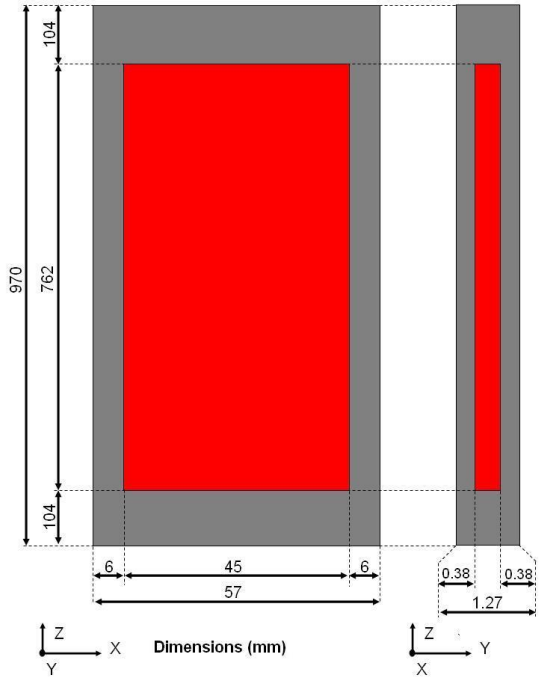

Figure 2 Schematic of the fuel plate and dimensions

2.2 Oxide Measurement Data from the BR2 experiments

Oxide thickness data of the E-FUTURE and SELENIUM plates were measured at locations where two dimensional power distribution is known. A schematic of the line-scans of oxide thickness measurement is shown in **Figure 3**. The oxide thickness data obtained by using an eddy current method equipped in the BONAPARTE measurement bench [8]. The measured oxide data were reported for 10 parallel lines along the plate axial length 5-mm apart from each other. The line 41 mm from the cold edge of the plate runs through the peak oxide thickness region near 500 mm from the top of the fuel meat, although the peak power occurred slightly more toward the meat edge. Because of cooling configuration, the peak cladding temperature occurred here.

Oxide measurements from the plate-ID side and non-ID side of each plate are presented in **Figure 4** - **Figure 6**, for 4111, 4202, and 6301 of the E-FUTURE experiment, respectively. The measured oxide thicknesses close to the peak plate swelling areas are in the range of 20 - 45 µm for all plates. The axially top and bottom parts of all plates have a flat oxide profile of 5 - 10 µm. The oxide thicknesses within the plate area with an extremely large swelling (around 500 mm from meat top) are exaggerated because the eddy current technique is highly sensitive to defects in the substrate material. In a small area near the pillowing region, the oxide appeared to have spalled off. This is probably related to the extensive swelling in the pillowed zone creating high local stresses in the oxide layer [8].

The visual inspection for the SELENIUM plates showed a darker color different from the typical oxide in high power regions. This might indicate that the oxide in these regions was at the onset of spalling. At such a high heat flux, the stress in an oxide layer ~35-μm thick may be high enough for cracks to develop. However, this oxide thickness is still smaller than the spallation criterion for SELENIUM plates, ~60 μm estimated using the criterion by Yoder [13]. Similar to the E-FUTURE experiment, the same line scan scheme was used. An oxide thickness profile of plate U7MD1221 for the line scan obtained at 41 mm marked in **Figure 3** is shown in **Figure 7** [9]. The maximum oxide thickness was about 45 μm in the peak power region.

Common to all plates, the oxide thickness data measured at 0 – 200 mm from the meat top are quite invariant and slightly decreasing along the scan direction, particularly so for the data along the scan line 51 mm. This is counter intuitive, considering that temperature and power rise along the scan direction. This might be due to unknown thermo-hydraulic irregularities occurring in the basket. In addition, the unrealistic negative readings along the 51 mm commonly shown for all plates are due to measurement difficulty because this line is over the meat edge where influence of the meat edge on the eddy currents is strong [8].

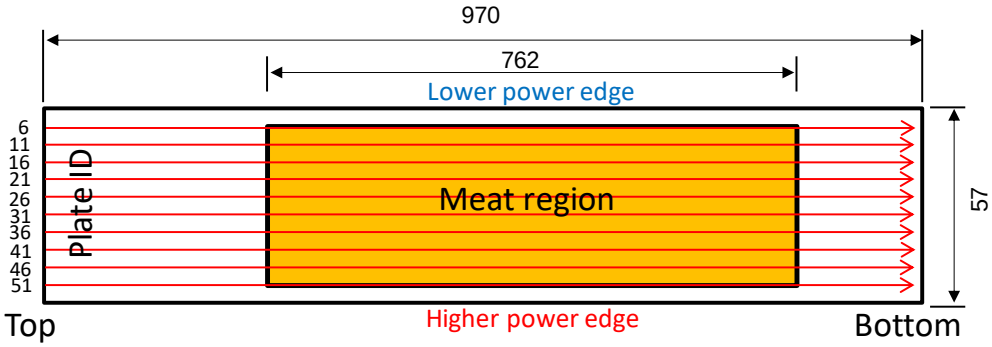

Figure 3 Schematic of oxide thickness measurement locations. The dimensions are in mm. The point of origin is at the upper right corner of the ID side of the plate.

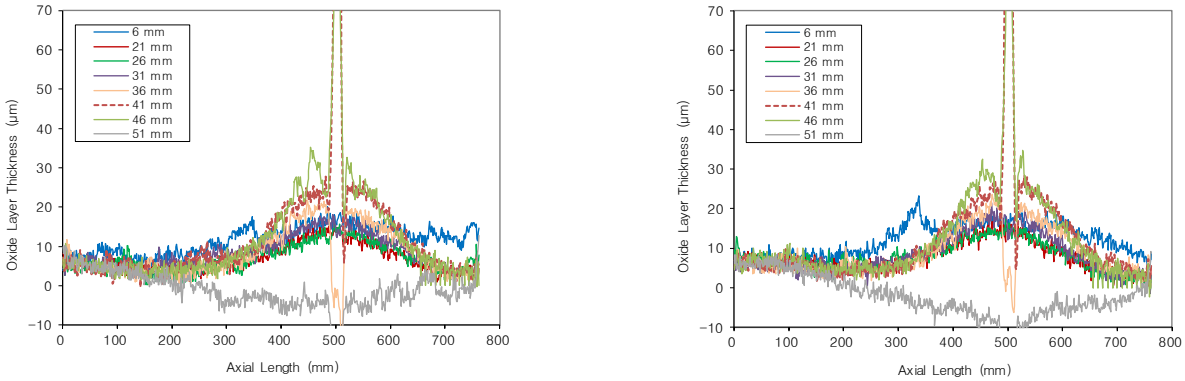

(a) Plate-ID side (b) Non-ID side

Figure 4 Oxide layer thickness data for the fuel plate 4111 of the E-FUTURE experiment

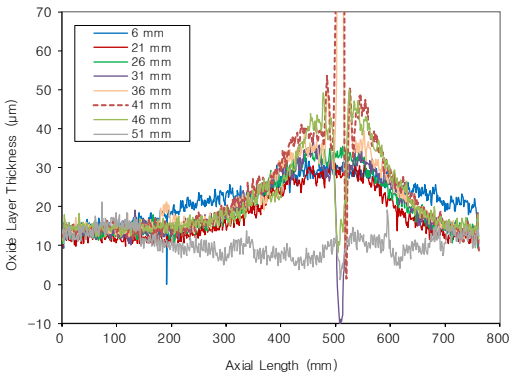

(a) ID side

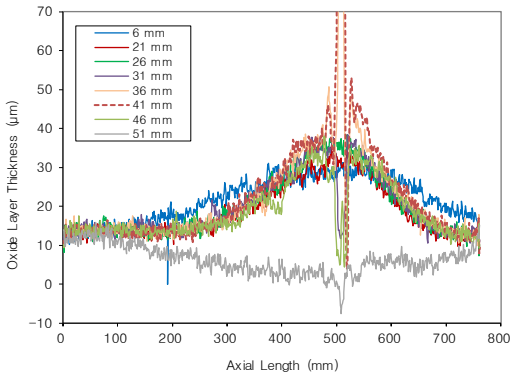

(b) Non-ID side

Figure 5 Oxide layer thickness data for the fuel plate 4202 of the E-FUTURE experiment

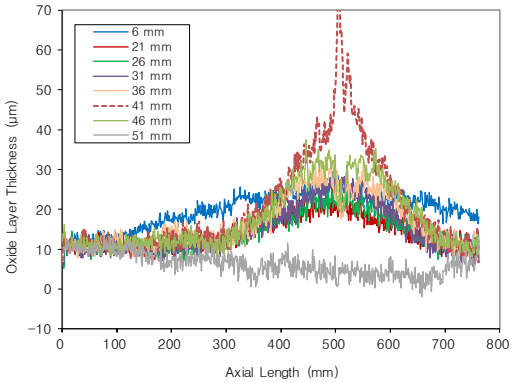

(a) ID side

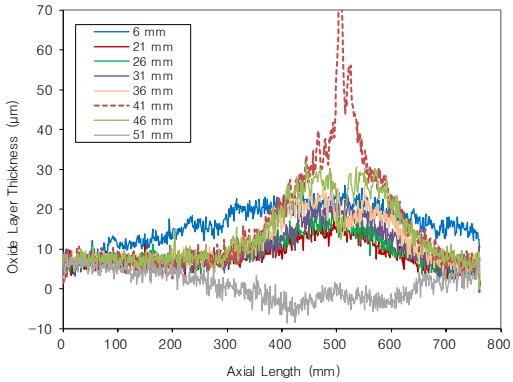

(b) Non-ID side

Figure 6 Oxide layer thickness data for the fuel plate 6301 of the E-FUTURE experiment

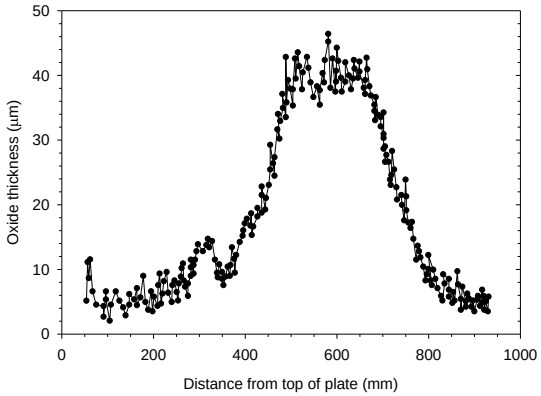

Figure 7 Oxide layer thickness data for the fuel plate 1221 of the SELENIUM experiment obtained along the 41 mm line from the lower power plate edge.

3. Cladding temperature prediction for BR2 experiments

3.1 Power distribution

The axial power distributions along the axial oxide measurement line 41 mm from the lower power side (see Figure 3) in the U7MC 4111, 4202 and 6301 fuel plates of the E-FUTURE experiment are taken from Ref. [14].This line is adjacent to the edge where the peak power occurs. Each cycle is divided into two subcycles in power and these time-dependent powers are used cladding surface temperature and oxide predictions. The E-FUTURE plates' powers are shown in **Figure 8**(a) –(c).

The axial power distribution of plate U7MD1221 of the SELENIUM experiment along the axial oxide measurement line 41 mm from the peak power side (see Figure 3) is given in **Figure 8**(d) [15].

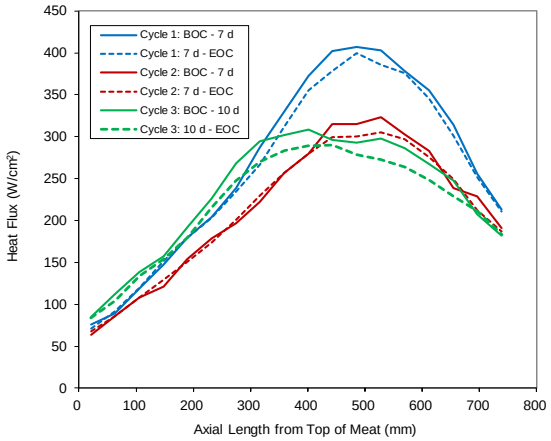

(a) E-FUTURE 4111

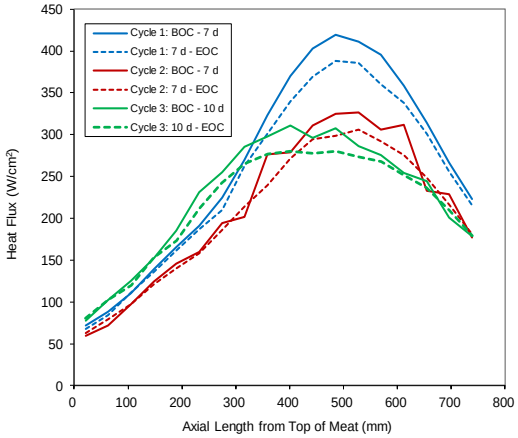

(c) E-FUTURE 6301

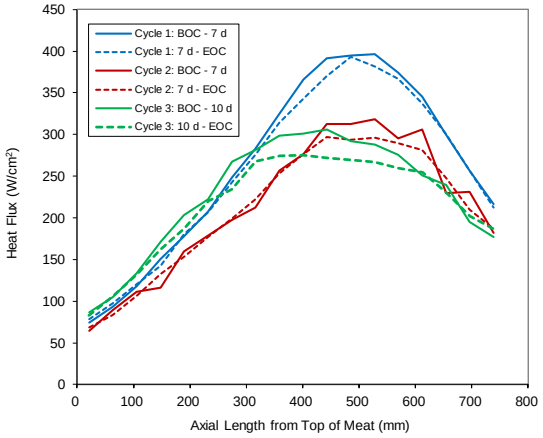

(b) E-FUTURE 4202

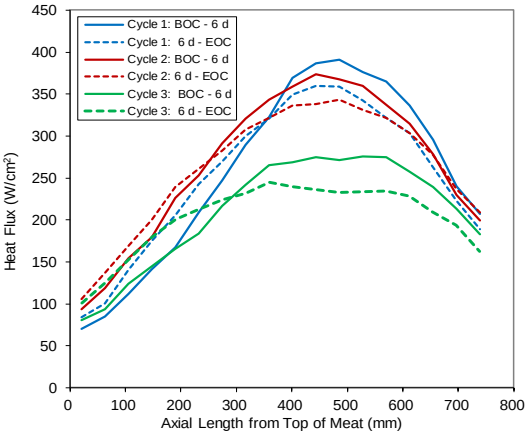

(d) SELENIUM 1221

Figure 8 Axial power distribution of the fuel plate 4111 along the axial line 41 mm from the lower power plate edge of the E-FUTURE experiment

3.2 Cladding surface heat transfer prediction

All of the experiments examined in this study had fluid velocities in the turbulent regime. Therefore, convection is the dominant mode of heat transfer. Applying Newton's law of cooling, the cladding surface temperature is calculated by

$$T_w = T_b + \frac{q}{ha} \tag{1}$$

where T_b is the bulk fluid temperature in K, q is the thermal power in W, h is the heat transfer coefficient (HTC) in W/(m^2-K) and a is the heated area in m^2. All values can be explicitly entered into Eq.(1) to calculate the cladding surface temperature for a particular set of appropriate boundary conditions.

Three correlations are most frequently used to calculate the HTC in plate type geometry. This group includes the Dittus-Boelter correlation [16], the Colburn correlation [17], and the Sieder-Tate correlation [18].

The Dittus-Boelter correlation is given by

$$Nu_{DB} = \frac{h\,D_e}{k} = 0.023\ Re_b^{0.8}\ Pr_b^{0.4} \tag{2}$$

where Nu, Re and Pr are the Nusselt, Reynolds and Prandtl numbers, respectively, evaluated at the bulk coolant temperature (T_b), D_e is the hydraulic diameter in m, and k is the coolant thermal conductivity in W/(m-K).

The Colburn correlation is

$$Nu_{CB} = 0.023\ Re_f^{0.8}\ Pr_f^{0.3} \tag{3}$$

where subscript f means the film temperature. The film temperature is the arithmetic mean of the bulk fluid and cladding surface temperatures.

The Sieder-Tate correlation is

$$Nu_{ST} = 0.027\ Re_b^{0.8}\ Pr_b^{1/3}\left(\frac{\mu_b}{\mu_w}\right)^{0.14} \tag{4}$$

where μ_b and μ_w are the dynamic fluid viscosities in N-s/m^2 evaluated at the bulk coolant and cladding surface temperatures.

The Dittus-Boelter correlation is recommended specifically for a situation in which the difference between cladding surface and fluid temperatures is small. The Colburn correlation is similar in form to the Dittus-

Boelter correlation but it considers the fluid properties at the film temperature. The Sieder-Tate correlation is similar to the Colburn correlation and is accurate for conditions with a large temperature difference between the cladding surface and the coolant temperatures because it is capable of explicitly incorporating the viscosities of the coolant at both the bulk coolant temperature and the cladding surface temperature.

At Korea Atomic Energy Research Institute (KAERI), HTC was measured in a rectangular channel, simulating the coolant channel of fuel plates [19]. It is worth noting that the KAERI correlation is based on plate channel data. The KAERI correlation takes the following form:

$$Nu_{KA} = 0.0058\, Re_b^{0.9383}\, Pr_b^{0.4} \tag{5}$$

3.3 Comparison of HTC correlations

In order to account for the changes in heat flux during a cycle, the total irradiation time was divided into time intervals consistent with those used in the physics calculation. The local power density during a time interval was converted to local heat flux to calculate surface temperature.

The four correlations discussed in sect. 3.2 were employed to calculate the HTC. The plate surface temperatures along the line passing through the peak oxide thickness location, 41 mm from the lower power edge of the plate, were calculated, using a revised version of the program developed at KAERI, Thermal Hydraulic Margin Calculator for Plate-type Fueled Reactor Core for Windows [20], which is an one-dimensional heat transfer equation solver. In order to compare the HTC correlations, the calculated Nusselt number along the plate length of the E-FUTURE 6301 plate is plotted in **Figure 9**(a). Also shown is the corresponding surface temperature in **Figure 9**(b).

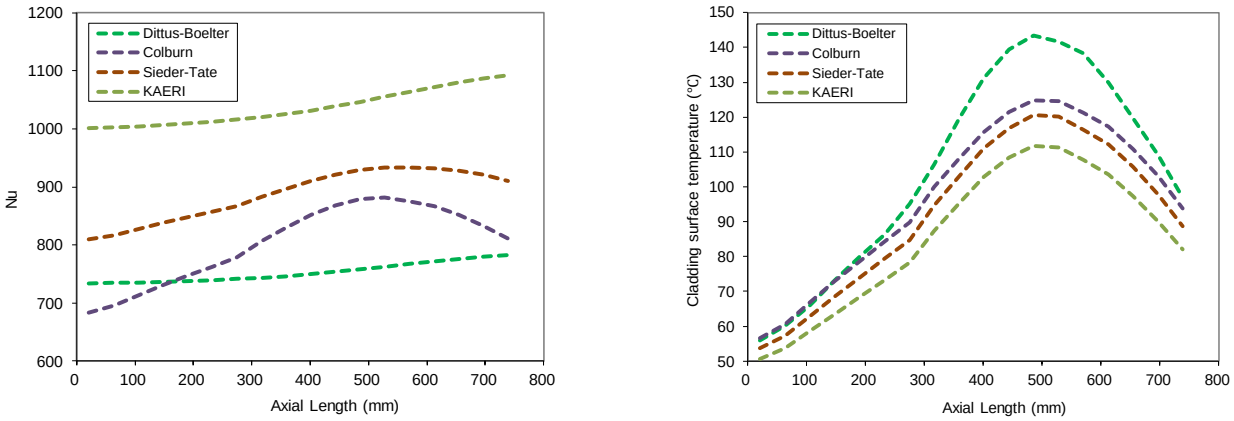

(a) Nusselt number (b) Cladding surface temperature

Figure 9 Comparisons of Nusselt number and cladding surface temperature between HTC correlations calculated along the axial line 41 mm from the lower power plate edge of the E-FUTURE 6301 plate at beginning of cycle 1.

The Dittus-Boelter correlation gave the highest cladding surface temperature. This result may be attributed to the model's inability to account for the difference in coolant viscosity at the cladding surface compared to the bulk coolant [21]. The greatest difference in the calculated maximum cladding surface temperature occurred at the axial position ~500 mm from the top of the plate. The largest difference in calculated temperature was ~30 ^{o}C between the predictions by the Dittus-Boelter and KAERI correlations.

4. Oxide prediction models

4.1 Griess model

The water-side oxide growth kinetics for Al cladding of research reactor fuel plates has long been calculated using the Griess model that was proposed by Griess in the 1960s. The Griess model was developed based upon out-of-pile data to predict the oxide growth of aluminum cladding in the High Flux Isotope Reactor (HFIR) and the Advanced Test Reactor (ATR) conditions. From the analysis of the test results, Griess derived the following correlation [1][2].

$$x = \begin{cases} 11{,}252 \exp\left(-\dfrac{4{,}600}{T}\right) t^{0.778}, & \text{for pH = 5.0} \\ 30{,}480 \exp\left(-\dfrac{4{,}600}{T}\right) t^{0.778}, & \text{for } 5.7 \le \text{pH} \le 7.0 \end{cases} \tag{6}$$

where x is the oxide layer thickness in μm, t is the time in h, and T is the cladding surface temperature in K. The unique difference of the Griess model compared to other oxide growth models is that it is independent of the effect of heat flux.

4.2 KAERI-modified Griess model

At KAERI, it was found that the Griess correlation over-predicted oxide growth when the heat flux was less than 3.18 MW/m^2. In the HANARO reactor, the effect of heat flux was measured and a correction factor (f_q) was determined to modify the Griess model [6]. The KAERI-modified Griess model takes the following form:

$$x = \begin{cases} 11{,}252 \exp\left(-\dfrac{4{,}600}{T}\right) t^{0.778} f_q, & \text{for pH = 5.0} \\ 30{,}480 \exp\left(-\dfrac{4{,}600}{T}\right) t^{0.778} f_q, & \text{for } 5.7 \le \text{pH} \le 7.0 \end{cases} \tag{7}$$

In Eq. (7), the correction factor is expressed by

$$f_q = \begin{cases} -0.20836 + 0.18915\, q, & \text{for 2.16 MW/m}^2 < q \\ 0.2, & \text{for } q < 2.16 \text{ MW/m}^2 \end{cases} \tag{8}$$

where q is the heat flux in MW/m^2.

4.2 Kim model

The Kim model comprises a series of equations empirically fit to measured data for AA 6061, predominantly at the ATR. A brief summary of the model from Ref. [7] is given below.

The rate equation for oxide growth is expressed by a power law:

$$\frac{dx}{dt} = k\, t^{-p} \tag{9}$$

where x, t, k, and p are the oxide thickness, time, reaction constant and rate-law power, respectively. The integration of Eq.(9) gives the following general form of the kinetics equation:

$$x = \left[x_0{}^{p+1} + (p+1)\, k\, t \right]^{\frac{1}{p+1}} \tag{10}$$

where x_0 is the oxide thickness at time zero.

The Kim model differs from other models in that the rate law power p varies due to degradation of the protective oxide layer. The aluminum alloy oxide dissolves in the water, controlled chiefly by coolant pH, temperature, and coolant velocity. The model's rate law power p is given by

$$\mathrm{p} = 0.12 + 9.22 \exp\left(-\frac{\mathrm{C_s}}{6.82 \times 10^{-9}} \right) \tag{11}$$

and the oxide solubility, C_s, is expressed by:

$$\mathrm{C_s} = \exp\left[-\left(-13.79 - \frac{1211.16}{\mathrm{T_{x/w}}} \right)\left(0.041\mathrm{H}^2 - 0.41\mathrm{H} - 0.07 \right) \right] \tag{12}$$

where $T_{x/w}$ is the temperature at the oxide-water interface and H is pH of the coolant. The applicable temperature range is 25 - 300 ^{o}C and pH not greater than 7.0.

The rate function k is expressed by an empirical formula:

$$\mathrm{k} = 3.9 \times 10^{5} \exp\left(\frac{-6071}{T_{x/w} + AB\frac{qx}{k_T}} \right) \tag{13}$$

where $T_{x/w}$ is the oxide-water interface temperature in K, q is the surface heat flux in MW/m^2, x is the oxide thickness in μm, k_T is the thermal conductivity of the oxide in W/m-K, A is the augmentation factor, and B is the correction constant, as described below.

A is added to the equation as a multiplier to take into account the effect of coolant velocity. The augmentation factor increases as the coolant velocity increases because of water ingress through the defective oxide. A is correlated with the coolant velocity using the following sigmoidal function:

$$A = 0.43 + \frac{3.21}{1 + \exp\left(-\frac{v_c - 13.39}{3.60}\right)} \tag{14}$$

where v_c is the coolant velocity in m/s. The applicable range of coolant velocity for this correlation is 3 ~ 28 m/s.

A correction constant, B, was needed to account for the reduction in the 'oxide thickness' caused by oxidant migration. The Kim model adopted B = 0.37 for AA 6061 and the ATR data.

The oxide thermal conductivity decreases as the oxide thickens. The effective oxide thermal conductivity was formulated as a function of the oxide thickness as follows:

$$k_T = 2.25, \qquad \text{for } x \le 25, \tag{15}$$

$$k_T = 2.25 - 0.016\,(x - 25), \qquad \text{for } 25 \le x \le 100 \tag{16}$$

where k_T is in W/m-K and x in μm, defined by Eq. (10).

5. Comparison of oxide model predictions for BR2 experiments

The three oxide prediction models described in the previous section were employed to calculate oxide thickness for the E-FUTURE and SELENIUM experiments conducted at BR2. The four HTC correlations were also parametrically used to calculate temperature for the oxide model calculations.

The oxide thicknesses predicted by the oxide growth models are compared with the measured data in **Figure 10 - Figure 13**. The experimental data points were averaged over 10 mm along the measurement line for the purpose of convenience. The measured data at the line scan 41 mm from the lower power edge of the plate were used for evaluation of the models. The 41-mm line runs through the peak oxide thickness region near 500 mm from the top of the fuel meat.

As can be seen in the figures, the calculated oxide thickness varies substantially depending on the applied HTC correlation. In general, the Griess model predicted the thickest oxide layer with all of the HTC correlations, and over-predicted the experimental data. The oxide predictions by the Kim model coupled with the Dittus-Boelter correlation diverged at the peak power region, implying that the Kim model is over-predicting at high temperatures. Except for the E-FUTURE 4111 with the Dittus-Boelter correlation and Colburn correlation, the KAERI-modified Griess model predicted the lowest oxide thickness of the oxide growth correlations with all HTC correlations.

When coupled with the Colburn correlation or the Sieder-Tate correlation, the Kim model was in fair agreement with the measured data. It may be due to the Colburn and Sieder-Tate correlations' ability to incorporate the coolant properties at the cladding surface so a better temperature prediction is possible than the Dittus-Boelter correlation. Between these two correlations, the Colburn correlation is slightly better because it more closely predicts the oxide thickness when combined with the Kim model. Therefore, in this study the Colburn correlation will be used for further revision of the Kim model.

For the axial locations in the 0 – 200 mm range, the measured data are higher than all oxide model predictions. As discussed in sect.2, this is attributed to the unknown thermo-hydraulic irregularities occurring in the basket.

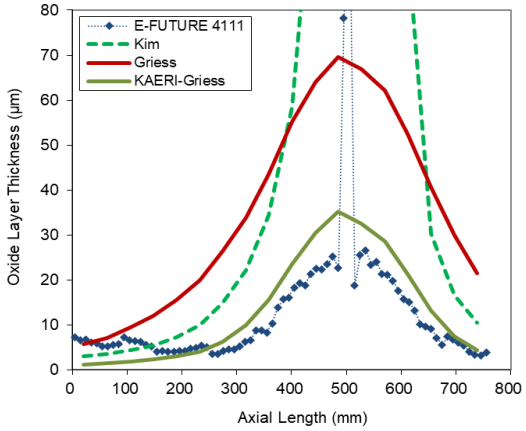

(a) The model predictions used HTC by the Dittus-Boelter correlation

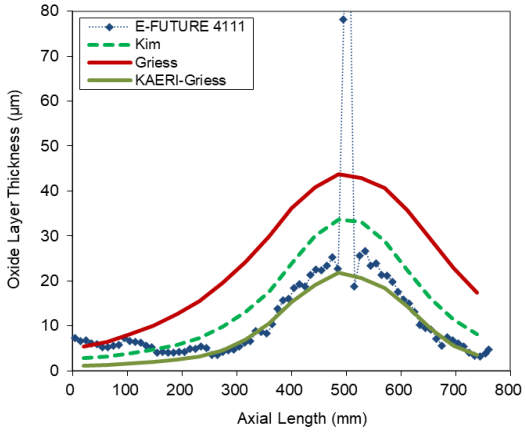

(c) The model predictions used HTC by the Sieder-Tate correlation

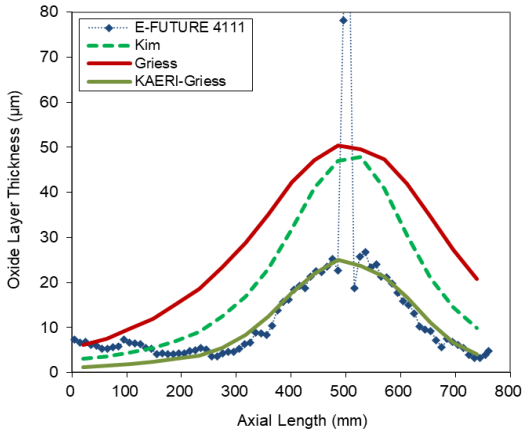

(b) The model predictions used HTC by the Colburn correlation

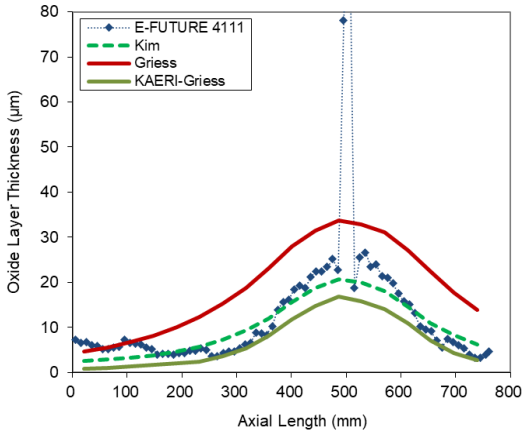

(d) The model predictions used HTC by the KAERI correlation

Figure 10 Comparison of the oxide thickness model predictions with the measured data for plate 4111 along the axial line 41 mm from the lower power edge of the E-FUTURE experiment.

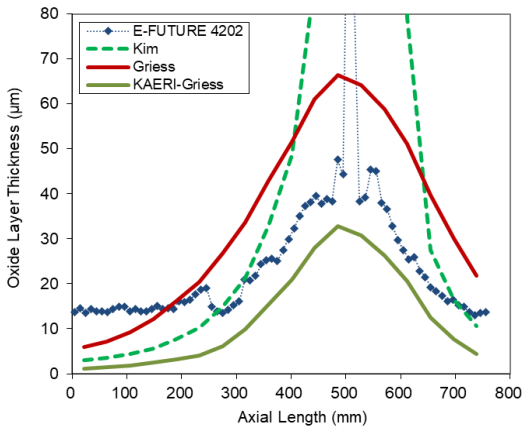

(a) The model predictions used HTC by the Dittus-Boelter correlation

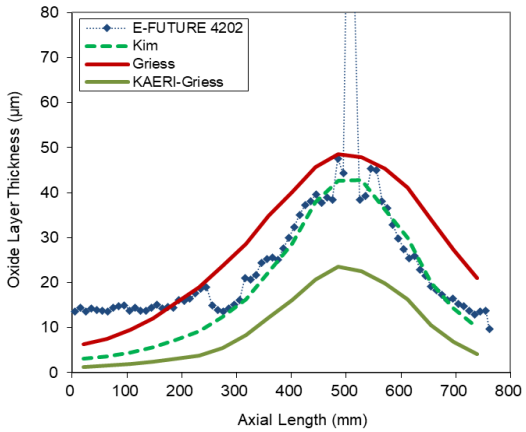

(b) The model predictions used HTC by the Colburn correlation

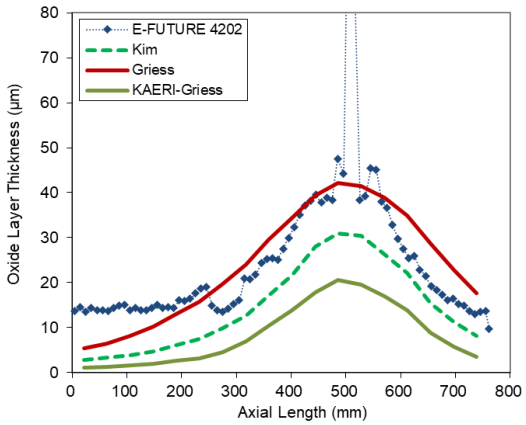

(c) The model predictions used HTC by the Sieder-Tate correlation

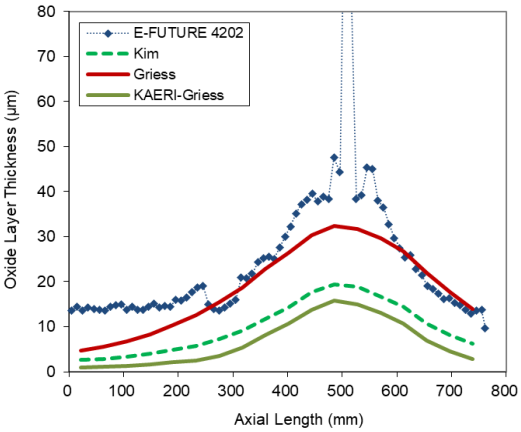

(d) The model predictions used HTC by the KAERI correlation

Figure 11 Comparison of the oxide thickness model predictions with the measured data for plate 4202 along the axial line 41 mm from the lower power edge of the E-FUTURE experiment

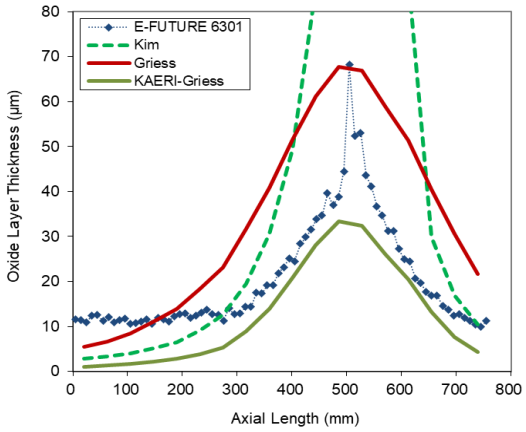

(a) The model predictions used HTC by the Dittus-Boelter correlation

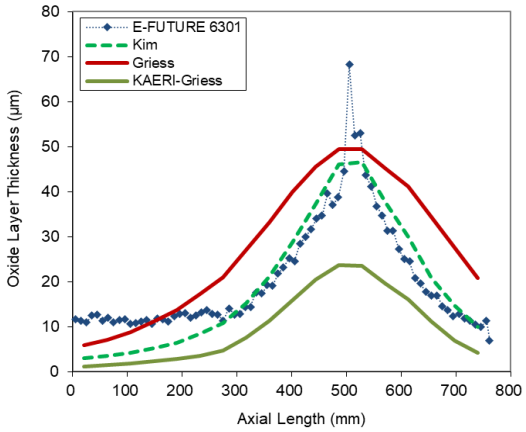

(b) The model predictions used HTC by the Colburn correlation

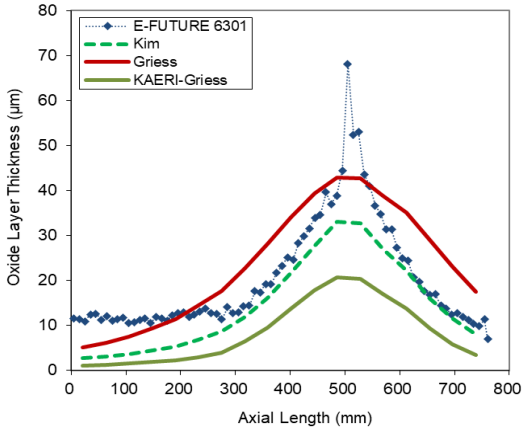

(c) The model predictions used HTC by the Sieder-Tate correlation

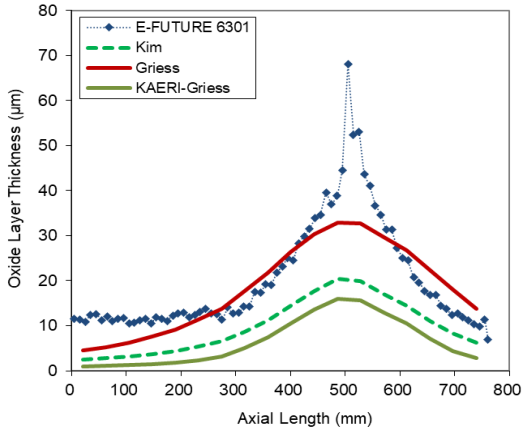

(d) The model predictions used HTC by the KAERI correlation

Figure 12 Comparison of the oxide thickness model predictions with the measured data for plate 6301 along the axial line 41 mm from the lower power edge of the E-FUTURE experiment

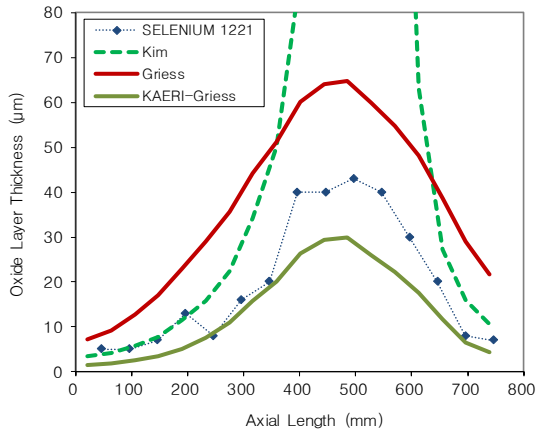

(a) The model predictions used HTC by the Dittus-Boelter correlation

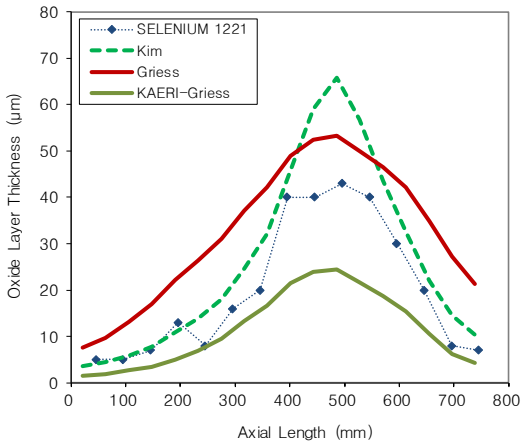

(b) The model predictions used HTC by the Colburn correlation

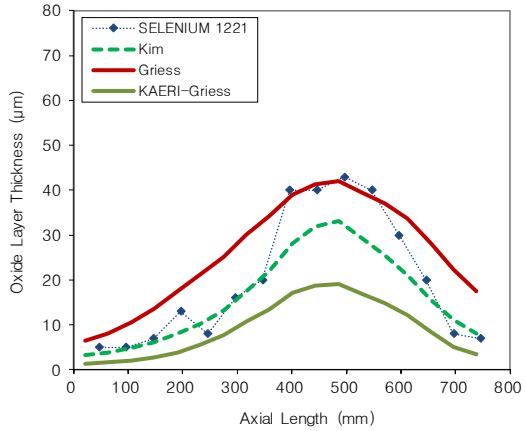

(c) The model predictions used HTC by the Sieder-Tate correlation

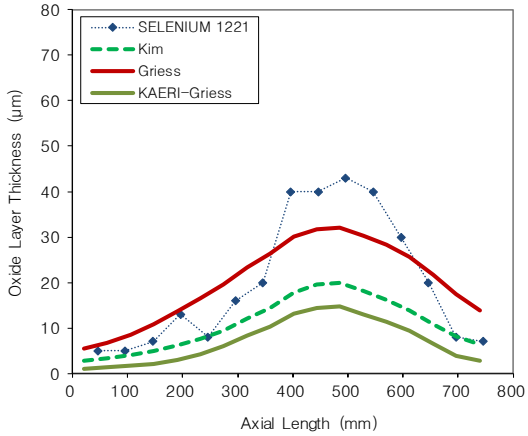

(d) The model predictions used HTC by the KAERI correlation

Figure 13 Comparison of the oxide thickness model predictions with the measured data for plate 1221 along the axial line 41 mm from the lower power edge of the SELENIUM experiment

6. Revision of the oxide prediction models for high flux research reactors

The Griess model generally over-predicted the oxide thickness, particularly for high temperature cases. Its inability to take into account the heat flux and pH is another disadvantage. Introducing a simple multiplication factor is not likely to improve its prediction accuracy. On the other hand, the KAERI-Griess model generally under-predicted the oxide thickness. This model was a revision from the Griess model built to incorporate a heat flux effect. However, it appears that the general over-prediction of the Griess model was over-corrected in the KAERI-Griess revision.

The Kim model extremely over-predicted for all plates at their respective peak power regions when it used temperatures predicted using HTC by the Dittus-Boelter HTC correlation (see **Figure 10 - Figure 13** part a). This result implies that the model is more temperature-sensitive more than the other models. The increase in oxide growth in peak power regions is so rapid that the oxide thickness prediction became divergent. The cause of this unrealistic increase is mainly due to the coupling of the rate constant and oxide thickness, which effectively feed back into itself, as the oxide thickness growth is dependent on the rate constant. Another drawback of this model is that the model requires a time step of 24 hours because of the coupling of the rate constant and oxide thickness. Therefore, the model predicts reasonably well for low power and low temperature conditions, but it is not applicable to high power and high temperature conditions. In order to overcome this disadvantage, a model revision was performed to remove the oxide thickness dependence on the rate constant using the E-FUTURE and SELENIUM test data together with other in-pile data given in **Table 2**.

Maintaining all other features unchanged, the rate constant was revised. The reaction constant has been rrevised as follows:

$$\mathrm{k} = 4.5 \times 10^{3} \exp\left(\frac{-4340}{T_{x/w} + A\dfrac{q}{k_T}} \right) \tag{17}$$

where A is the constant given by Eq.(14) and all other variables preserve the earlier definitions. Comparing with Eq.(13), oxide thickness x is removed from the reaction rate constant. In addition, the constant B which was necessary to adjust for the reactor-dependent coolant channel geometry is now removed.

Figure 14 compares the oxide predictions by the revised Kim model and the original Kim model with the SELENIUM data. There is no more divergence in peak power regions when the revised model used temperatures predicted by the Dittus-Boelter HTC correlation. For other HTC correlations, both models predict close to each other. It is judged that the best result is found when the model is coupled with the Colburn correlation. **Figure 15** compares the oxide predictions by the revised Kim model and the original Kim model coupled with the Colburn HTC correlation for the E-FUTURE test plates. Both model predictions are close to each other. This suggests that the revised Kim model predicts consistently with the original Kim model while removing the divergence for high temperature cases. The revised model coupled with the Colburn correlation also compares well with the measured for other data (see **Table 2**).

If other HTC correlations are to be used, the pre-exponential constant in Eq.(17) must be adjusted accordingly. For other HTC correlations, the best pre-exponential constants were obtained and given in **Table 3**.

Considering the ranges of the data used for the data fit, the revised model is applicable for cladding surface temperature in the range of $25 \le \mathrm{T} \le 160\,^{\circ}\mathrm{C}$, for pH $5.0 \le \mathrm{pH} \le 7.0$, and for coolant speed $3.0 \le \mathrm{v}_c \le 20.0$ m/s.

Table 2 In-pile oxide data used for data fit and model predictions

	Time (d)	Temp [a] (^oC)	Heat flux (MW/m^2)	pH	Coolant speed (m/s)	Measured Oxide (μm)	Ref. for measured data	Griess	KAERI-Griess	Original Kim [7]	Revised Kim
UMUS LEU 90mm	48	82.6	1.7	6.5	8.3	16 ± 5	[22]	18	4	14	18
SIMONE LC-04	153	72	0.79	6.5	6.6						
	141	56	0.43	6.5	6.6						
	102	59	0.47	6.5	6.6						
	72	53	0.35	6.5	6.6						
	23	67	0.68	6.5	6.6	43 ± 7	[7]	41	8	34	50
UMUS MEU 274mm	48	107.4	2.5	6.5	8.3	61 ± 7	[22]	41	11	57	40
ORR A101	19	96	1.92	5.2	8.5						
	15	95	1.90	5.4	8.5						
	35	89	1.80	5.6	8.5						
	18	88	1.76	5.9	8.5						
	33	81	1.58	6.1	8.5						
	27	79	1.58	6.3	8.5	14 ± 2	[7]	45	9	9	11
FUTURE right plate	10	113	3.20	6.2	12						
	10	111	3.03	6.2	12						
	10	109	2.86	6.2	12						
	10	106	2.69	6.2	12	21 ± 3	[7]	47	16	23	22
E-FUTURE 4202 [b]	26	120	3.7	6.2	12						
	28	108	3.1	6.2	12						
	20	103	2.8	6.2	12	36 ± 2	[23]	59	23	39	39
RERTR-7A B7	20	102	2.30	5.2	10.8						
	20	101	2.25	5.2	10.8						
	20	99	2.20	5.2	10.8						
	20	97	2.15	5.2	10.8						
	10	94	2.10	5.2	10.8	6 ± 1.0	p	53	11	5	5

a: The Colburn correlation was used.

b: At 41 mm from the lower power side edge and 450 mm from the top edge of the plate (see Figure 3). This location was selected to avoid the pillowed region where the oxide measurement might be inaccurate.

p: present study

Table 3 Proposed pre-exponential constant in Eq.(17) for each HTC correlation when used with the revised Kim model

HTC correlation	Pre-exponential constant in Eq.(17)
Dittus-Boelter	3.2×10^{3}
Colburn	4.5×10^{3}
Sieder-Tate	5.8×10^{3}
KAERI	9.5×10^{3}

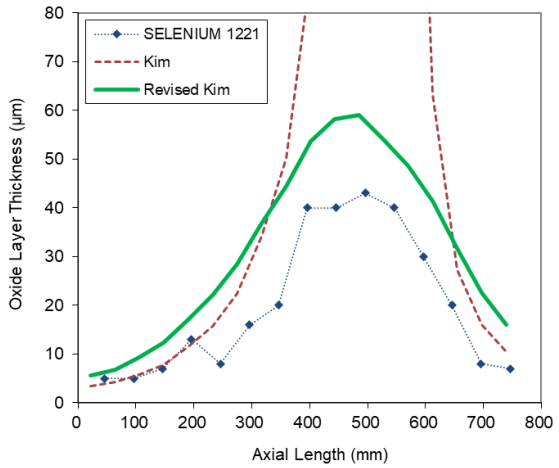

(a) The model predictions used HTC by the Dittus-Boelter correlation

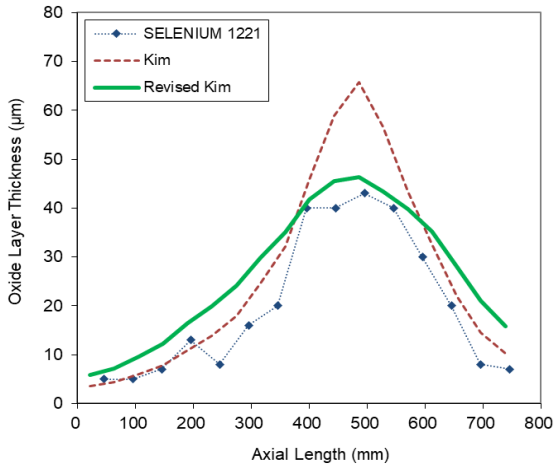

(b) The model predictions used HTC by the Colburn correlation

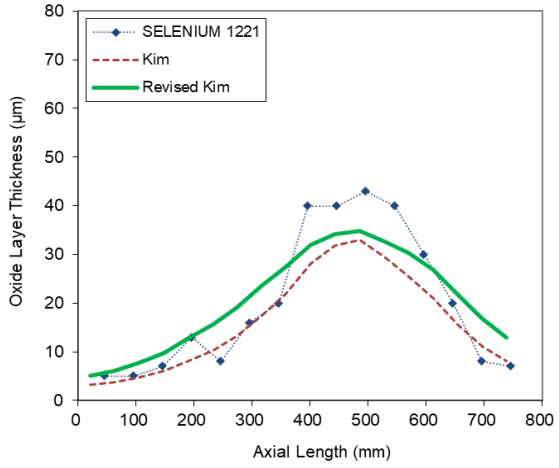

(c) The model predictions used HTC by the Sieder-Tate correlation

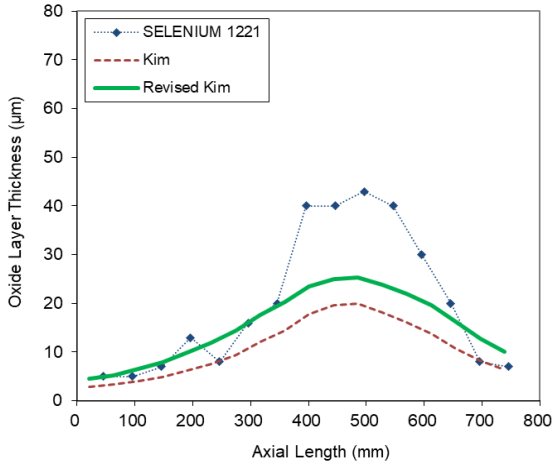

(d) The model predictions used HTC by the KAERI correlation

Figure 14 Comparison of oxide thickness prediction by the revised Kim model with the original model and the measured data along the axial line 41 mm from the lower power edge of the SELENIUM 1221 plate

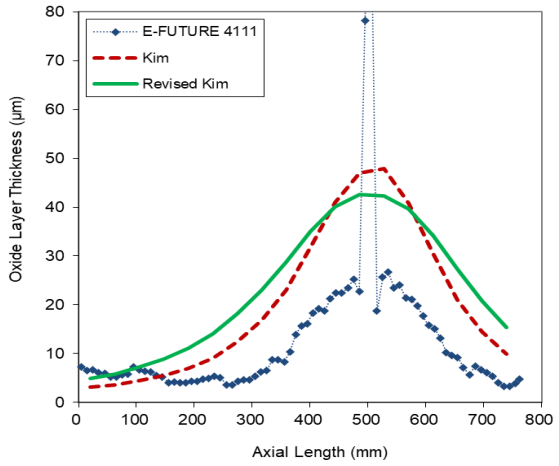

(a) E-FUTURE plate 4111

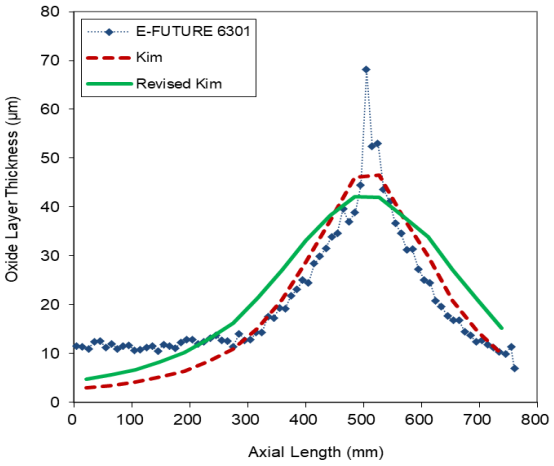

(c) E-FUTURE plate 6301

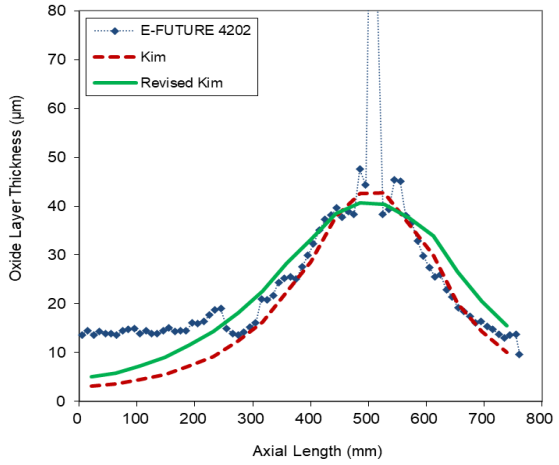

(b) E-FUTURE plate 4202

Figure 15 Comparison of oxide thickness prediction by the revised Kim model with the original model and the measured data along the axial line 41 mm from the lower power edge of the E-FUTURE test plates. The Colburn HTC correlation was used for all predictions.

7. Effect of Cladding Type

Because the cladding materials of the E-FUTURE and SELENIUM tests in the BR2 were AG3NE (closest to AA5754) and AlFeNi Al-alloys, different from the AA6061 cladding the Kim model was based upon, one might expect an effect of cladding alloy types on the oxide growth (see a comparison of the nominal compositions of these three alloys in **Table 4**).

In order to investigate the effect of cladding type, the oxide thickness data of the E-FUTURE plates with AG3NE and AlFeNi were compared, as shown in **Figure 16**. The E-FUTURE 4111 plate made with AlFeNi, in general, showed lower oxide growth than that of the E-FUTURE 6301 plates made with AG3NE.

From this result, because the 4111 plate was irradiated at only a slightly lower power than the 6301 plate, and all other irradiation conditions were virtually identical, the generally lower oxide thickness of the 4111 plate (a maximum of ~5 μm oxide thickness at locations away from the pillowed region) indicates that AlFeNi cladding is slightly advantageous over AG3NE. This result is an outlier compared to findings in the literature [7][24][25]. A possible reason for this discrepancy may be attributed to the higher temperatures for the BR2 test compared to those in the literature. Like a magnifying glass, the high temperature test magnifies the difference that was not discernable in the low temperature tests. However, it is these authors' belief that this effect is less important, at the most a secondary effect, than that of coolant conditions on oxide thickness. Therefore, in the present study a detailed discussion on the impact of cladding type on oxide growth is not included. The uncertainties in pH, coolant velocity, and reactor power are likely larger than the effect of cladding type.

Table 4 Compositions (wt.%) of aluminum cladding alloys

Alloy	Si	Fe	Cu	Mn	Mg	Cr	Ni	Zn	Zr	Ti	Other unspecified (max)	
											each	total
AlFeNi	0.3 Max	0.8-1.2	0.008 max	0.2-0.6	0.8-1.2	0.2-0.5	0.8-1.2	0.03 max	0.06-0.14	0.02-0.08	0.03	0.5
AG3NE	0.3 max	0.2-0.40	0.008 max	0.7 max	2.5-3.0	0.3 max	-	0.03 max	-	0.02 max	0.03	0.15
AA6061	0.4-0.8	0.70 max	0.15-0.40	0.15 max	0.8-1.2	0.04-0.35	-	0.25 max	-	0.15 max	0.05	0.15

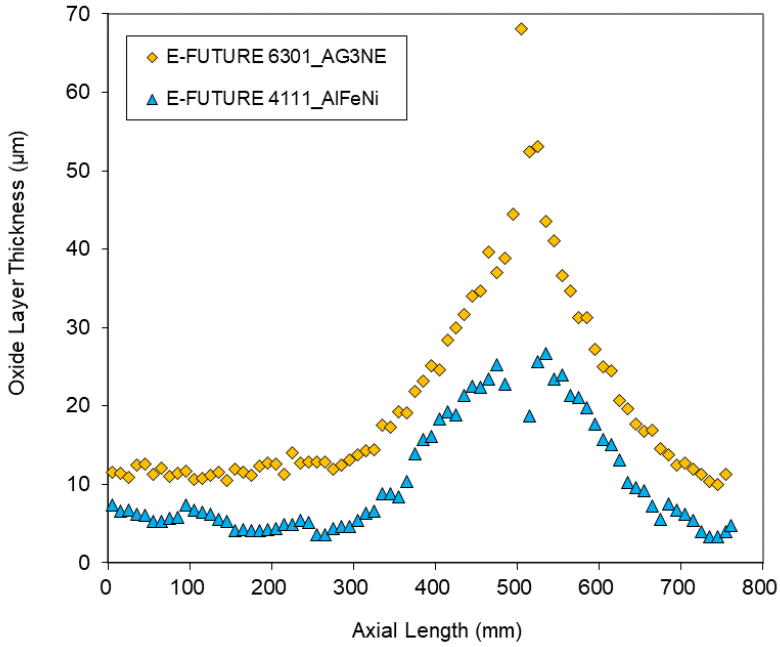

Figure 16 Comparison between AG3NE and AlFeNi cladding types tested in the E-FUTURE

8. Conclusions

The E-FUTURE and SELENIUM experiments at the BR2 were performed under high power densities and high cladding temperatures prevailed. The high heat flux and cladding temperature were beyond the conditions of the database used to develop the currently available oxide prediction models. To examine the applicability of the currently available models to these BR2 test conditions, the oxide prediction models including the Griess model, KAERI-modified Griess model and Kim model were studied coupled with the most frequently employed heat transfer coefficient (HTC) correlations including the Dittus-Boelter correlation, the Colburn correlation, the Sieder-Tate correlation, and KAERI-developed correlation.

The Griess oxide prediction model over-predicts for all test plates and for all HTC correlations. The KAERI-Griess model generally under-predicted.

The Dittus-Boelter HTC correlation led to predict higher cladding surface temperatures than the other correlations, resulting in higher oxide thickness predictions for all oxide thickness prediction models. The KAERI HTC correlation predicted the lowest temperatures among the HTC correlations compared, so lower oxide predictions were obtained.

The Kim model, when using the Colburn correlation for temperature calculations, gave the most consistent results with the measured data. However, the Kim model was found to be inapplicable to the EUHFRR test conditions at peak power locations if it is coupled with the Dittus-Boelter correlation, as the correlation

diverged. A revision of the rate function of the model, preserving other variables, was made. The revised Kim model showed more consistent predictions for high power and temperature conditions for all HTC correlations as well as low power conditions.

The prediction models in the literature were developed on data obtained mostly for AA6061 cladding whereas the EUHFRR including the BR2 tests use AG3NE and AlFeNi cladding. The difference in cladding alloy type was not considered in the formulation of the oxide growth models. Examination of the E-FUTURE test plates revealed that a noticeable difference, although small, exists between AG3NE and AlFeNi. Use of AlFeNi cladding appears to result in slightly thinner oxides. However, this difference was believed to be only a secondary effect considering other uncertainties in the model predictions. Hence, no attempt to model the alloying effect on oxide thickness was made for the revised model.

Acknowledgments

This work was supported by the U.S. Department of Energy, National Nuclear Security Administration (NNSA), Office of Material Management and Minimization (NA-23) Reactor Conversion Program under Contract No. DE-AC-02-06CH11357 between UChicago Argonne, LLC and the US Department of Energy.

Data availability statement

The raw/processed data required to reproduce these findings cannot be shared at this time as the data also forms part of an ongoing study.

References

[1] J.C. Griess, H.C. Savage, J.L. English, Effect of heat flux on the corrosion of aluminum by water. Part IV. Tests relative to the Advanced Test Reactor and correlation with previous results, Report, ORNL-3541, 1964.

[2] J.C. Griess, H.C. Savage, J.G. Rainwater, T.H. Mauney, J.L. English, Effect of heat flux on the corrosion of aluminum by water. Part III. Final report on tests relative to the High Flux Isotope Reactor, ORNL-3230, Oak Ridge National Laboratory, 1961.

[3] R.S. Ondrejcin, Evaluation of Mark 22 cladding, DPST-83-324, Savannah River Laboratory (1983).

[4] R.E. Pawel, G.L. Yoder, D.K. Felde, B.H. Montgomery, M.T. Mcfee, 36(1/2) (1991) 175.

[5] R.E. Pawel, D.K. Felde, J.A. Clinard, T.A. Thornton, Corrosion 93 (1993) 188/1.

[6] C.B. Lee, D.S. Sohn, Evaluation of the Corrosion Behavior of the Aluminum Cladding in the KMRR Fuel, J. Korean Nucl. Soc. 26 (4) (1994) 526.

[7] Yeon Soo Kim, G.L Hofman, A.B. Robinson, J.L. Snelgrove, N. Hanan, J. Nucl. Mater. 378 (2008) 220.

[8] S. Van den Berghe, Y. Parthoens, F. Charollais, Yeon Soo Kim, A. Leenaers, E. Koonen, V. Kuzminov, P. Lemoine, C. Jarousse, H. Guyon, D. Wachs, D. Keiser Jr, A. Robinson, J. Stevens, G. Hofman, J. Nucl. Mater. 430 (2012) 246.

[9] S. Van den Berghe, Y. Parthoens, G. Cornelis, A. Leenaers, E. Koonen, V. Kuzminov, C. Detavernier, J. Nucl. Mater. 442 (2013) 60.

[10] B. Ye, J. Rest, Yeon Soo Kim, G. Hofman, B. Dionne, Nucl. Technol. 191 (2015) 27.

[11] V. Marelle, F. Huet, P. Lemoine, Thermo-mechanical modelling of U-Mo fuels with MAIA, Trans. Intern. Meeting Research Reactor Fuel Management (RRFM), ENS, Munich, Germany, Mar. 21-24, 2004.

[12] S. Valance, A. Monnier, H. Palancher, B. Ye, A. Yacout, Benchmarking of the MTR fuel simulation codes DART and MAIA, Trans. Intern. Meeting Research Reactor Fuel Management (RRFM), ENS, Crowne Plaza Dead Sea Resort, Jordan, Mar. 24 -28, 2019.

[13] G.L. Yoder, N.C.J. Chen, D.K. Felde, W.R. Nelson, R.E. Pawel, Nucl. Eng. Des. 136 (1992) 401.

[14] V. Kuzminov, E. Koonen, "Qualification irradiation of new high density UMo LEU fuel plates and operating conditions during irradiation at the BR2 high flux materials testing reactor," Trans. Intern. Meeting Research Reactor Fuel Management (RRFM), ENS, Rome, Italy, Mar. 20 -24, 2011.

[15] V. Kuzminov, "SELENIUM Test Irradiation. Evaluation of Irradiation Conditions for Two UMo LEU SELENIUM Fuel Plates during the BR2 Cycles 02/2012 – 04/2012," Report, SCK·CEN-R-5639. Revision 1, SCK-CEN, January 2013.

[16] F.W. Dittus, L.M.K. Boelter, "Heat transfer in automobile radiator of the tubular type," University of California at Berkley Publ. Eng. 2, 443-461, 1930.

[17] A.P. Colburn, Trans. AIChE J. 29 (1933) 174.

[18] E.N. Sieder, G.E. Tate, Indust. Eng. Chem. 28 (1936) 1429.

[19] D.S. Jo, O.S. Al-Yahia, R.M. Tamimi, J.H. Park, H.T. Chae, Nucl. Eng. Technol. 46(2) (2014) 195.

[20] H.M. Sohn, "User manual of TH_Calc Win 1.0a," Report in Korean, KAERI Report, 2017.

[21] W.R. Marcum, D.M. Wachs, A.B. Robinson, M.A. Lillo, J. Nucl. Mater. 471 (2016) 136..

[22] A. Languille, D. Planco, F. Huet, B. Guigon, P. Lemoine, P. Sarristan, G.L. Hofman, J.L. Snelgrove, J. Rest, S.L. Hayes, M.K. Meyer, H. Vacelet, E. Leborgne, D. Dassel, Intern. Meeting Research Reactor Fuel Management (RRFM), Ghent, Belgium, Mar. 17-20, 2002.

[23] F. Frery et al., "LEONIDAS UMo Dispersion Fuel Qualification Program: Progress and Prospects," Proceedings of the 32nd International Meeting on Reduced Enrichment for Research and Test Reactors, Lisbon, Portugal, Oct. 10-14, 2010.

[24] E. Shaber, G.L. Hofman, "Corrosion minimization for research reactor fuel," INL/EXT-05-00256, Idaho National Laboratory, 2005.

[25] K. Farrell, "Performance of Aluminum in Research Reactors." In: R.J.M. Konings, (ed.) Comprehensive Nuclear Materials, Vol. 5, pp. 143-175 Amsterdam: Elsevier, 2012.